NASA TECHNICAL NOTE NASA TN D-3187

NASA TN D-3187

FEASIBILITY OF ACCELERATING MICRON-SIZE PARTICLES IN SHOCK-TUBE FLOWS FOR HYPERVELOCITY DEGRADATION OF REFLECTIVE SURFACES

by Michael J. Mirtich and Herman Mark

Lewis Research Center
Cleveland, Ohio

NATIONAL AERONAUTICS AND SPACE ADMINISTRATION • WASHINGTON, D. C. • JANUARY 1966

NASA TN D-3187

FEASIBILITY OF ACCELERATING MICRON-SIZE PARTICLES IN SHOCK-TUBE FLOWS FOR HYPERVELOCITY DEGRADATION OF REFLECTIVE SURFACES

By Michael J. Mirtich and Herman Mark

Lewis Research Center
Cleveland, Ohio

NATIONAL AERONAUTICS AND SPACE ADMINISTRATION

For sale by the Clearinghouse for Federal Scientific and Technical Information
Springfield, Virginia 22151 – Price $2.00

FEASIBILITY OF ACCELERATING MICRON-SIZE PARTICLES IN SHOCK-TUBE FLOWS FOR HYPERVELOCITY DEGRADATION OF REFLECTIVE SURFACES

by Michael J. Mirtich and Herman Mark

Lewis Research Center

SUMMARY

The feasibility of using short-duration shock-tube flows to accelerate micron-size particles of known mass and composition to hypervelocities has been studied both analytically and experimentally. Analytic studies that use the Stokes drag law corrected for slip flow by the semiempirical Cunningham-Millikan correction factor were made for various shock Mach numbers to 30, and the character of the acceleration problem was outlined. Experimental studies were made by accelerating micron-size particles to Mach 13 in a 2.9-inch shock tube. These studies demonstrated that short-duration shock-tube flows could be used as a means of accelerating micron-size particles for exposing surfaces to hypervelocity impact. Optical properties of these exposed surfaces were quite reproducibly affected by exposure, and an analytical model of the surface degradation phenomenon satisfactorily related measured reduction of surface reflectance with the total energy of impinging particles. The analysis suggested a means of using accurate measurements in the laboratory to predict reflectance degradation for surfaces under actual meteoroid dust exposure in space.

INTRODUCTION

The difficulty of providing accurate estimates of the performance of space vehicle components under the unusual conditions of the space environment can be reduced by studying the effects of these conditions in ground facilities wherein the environment has been simulated. Among the numerous facilities built for this purpose over the last few years none has so far included the capability of providing simulation of the meteoroid

environment. The difficulty of providing such a capability exists first because of an incomplete knowledge of this environment. Also, there has been a lack of satisfactory methods for accelerating known size particles to the required relative speeds at impact with the target.

Since the dangers to space travel of this meteoroid feature of the space environment are well recognized, many efforts have been made, instead, to study the phenomenon of the encounter of a single particle, moving at meteoric speeds, with a target representing a vehicle surface or component wall. The purpose of such studies has invariably been the determination of the penetration laws for such encounters with the express goal of protecting various types of fluid containers from catastrophic puncture. Data compiled from many space experiments (refs. 1 and 2) indicate, however, that the frequency of encounter with meteoroids will increase very rapidly as the mass of the meteoroid particle decreases. For meteoroid particle mass below that which might be considered a penetration hazard, the measured flux has increased so much that the primary space flight problem due to these smaller meteoroids becomes one of surface erosion and the subsequent modification of the optical properties of the eroded surfaces. It is clear that a device which could provide quantitative and reproducible exposure of surfaces to high-speed micron-size particles could be useful in studying the micrometeoroid erosion problem, and it was with this purpose in mind that a program to develop such a facility was initiated.

The short-duration flows of high-speed high-temperature gas in a shock tube have been used extensively to provide the environment necessary for the study of the problems of hypersonic flight. The possibility of using the aerodynamic drag of such gas flows as a means of accelerating small particles of known mass and composition to shocked gas speeds seemed worthwhile to investigate because such an investigation could be based on this strong aerodynamic foundation. It would only involve, therefore, the problem of outlining the regions of flow in the shock tube where small particles could be usefully accelerated. An evaluation of the method of exposing targets to particles accelerated in this way could follow, hopefully allowing the development of a ground facility which would remove the need for subjecting every material or surface of interest to actual space exposure.

Thus, a program was initiated at the Lewis Research Center to evaluate the use of shock tubes for accelerating small particles of known mass and composition to high speeds, and further to impact these high-speed particles against target surfaces for the purpose of studying quantitatively the effect of such exposure on the optical properties of these target surfaces. The studies made were both experimental and analytical. The experimental studies were made for various types and size ranges of particles for shock Mach numbers in air ranging from 6.0 to 13.0. The analytic studies were extended to Mach 30 in an effort to predict the velocities of various size particles for gas speeds up

to 30 000 feet per second in flow durations as short as 27 microseconds. The development of the experimental methods and the results of these experimental and analytical studies are presented herein.

ACCELERATION OF PARTICLES

The environmental conditions encountered by a particle in a shock tube can be illustrated by the wave-particle diagram presented in figure 1. The tube consists of two chambers, high pressure and low pressure, separated by a diaphragm. When the diaphragm opens, compression waves, which rapidly steepen into a shock wave, move into the low-pressure region, region 1. At the time the diaphragm opens, an expansion wave propagates into the high-pressure driver gas, region 4, reflects off the back wall of the driver section, and propagates into the low-pressure chamber. The surface that separates the driven gas from the driver gas is referred to as the contact surface. Across this surface the velocity and pressure are equal, but the temperature and density are not in general equal for the two gases. (The temperature of the driven gas, air, at the conditions presented in this report varies between 2820° and 10 875° K.) Particles placed in the middle of the low-pressure chamber at some distance downstream of the diaphragm are accelerated by the driven gas, region 2, and some heavier ones that are not as yet at gas speed on arrival of the contact surface fall behind and are accelerated by the cold expanded driver gas, region 3, until the termination of flow, assumed here to be the arrival of the first expansion wave. It is sometimes desirable to have the particles pass behind the contact surface and continue to be accelerated by the cold flow in region 3 if the melt-

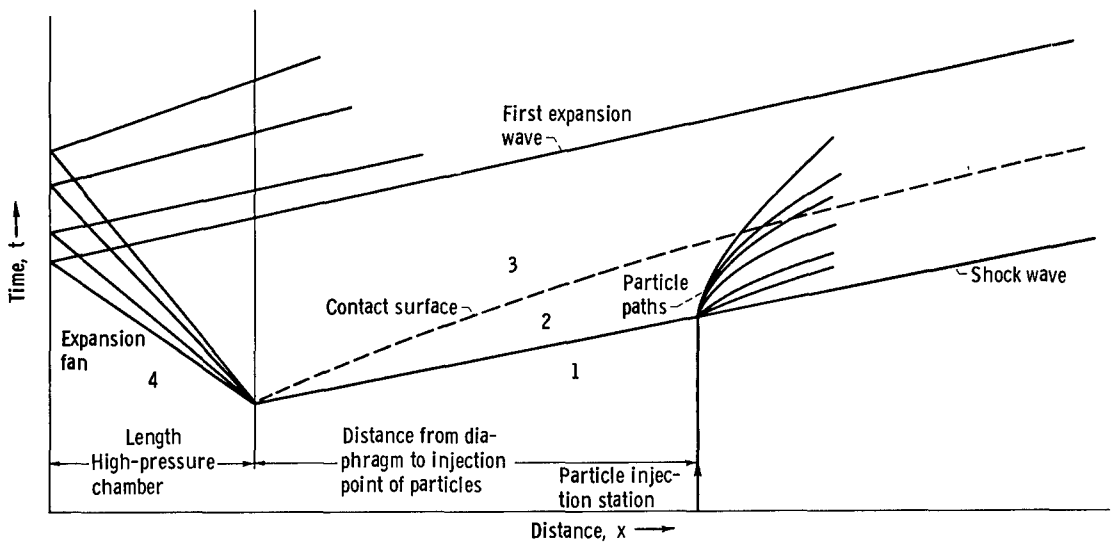

Figure 1. - Wave-particle diagram for constant area shock tube.

ing or sublimation temperature of the particles is less than the hot gas temperature of region 2 (since this can produce an undesirable ablating particle).

With the preceding flow picture in mind, an analysis was made to determine the feasibility of accelerating particles with these short-duration shock-tube flows. The accelerating force was assumed to be the aerodynamic drag of the high-speed gas acting on spheroidal particles placed in the stream. It was also assumed that the time for particle pickup at the injection station was small, and calculations showed that the Reynolds numbers for the particles relative to the gas would be low during a large part of the accelerating process. These low Reynolds numbers would allow use (thus giving conservative drag estimates) of the well-known Stokes solution for spheres. Stokes drag has been used by many investigators in the past and is used here essentially to show the character of the acceleration problem in a shock tube. In this case the drag force is given by the following equation (see appendix A for definition of symbols):

$$f_d = 3\pi\eta D(V_g - V_p) \tag{1}$$

Now the Stokes drag law is valid up to the limitations imposed by the phenomenon of slip. This phenomenon becomes important when the particle diameter is of the same order of magnitude as the mean free path of the molecules of the gas in which the particles are suspended. A correction for slip (ref. 3) was made by putting the semiempirical Cunningham-Millikin correction factor k_m in the denominator of the right side of equation (1). For air k_m is defined by the following equation:

$$k_m = 1 + \frac{0.16\times10^{-4}\,\text{cm}}{D}\,\frac{T}{T_o}\,\frac{P_o}{P} \tag{2}$$

where P_o and T_o are the conditions at standard temperature and pressure (STP). If D, the diameter of the particle, becomes large enough to make the second term in equation (2) much less than 1, there is no correction for slip flow. Since conditions in a shock tube are such that, at times, the mean free path of the accelerating gas approaches the particle diameter, k_m was added to give a conservative estimate of the acceleration process. Hence, if spheroidal particles are assumed, equation (1) can be rewritten as:

$$-\frac{f_d}{m_p} = \frac{d}{dt}(V_g - V_p) = -K(V_g - V_p) \tag{3}$$

where

$$K = \frac{b}{m_p} = \frac{18\eta}{k_m \rho D^2}$$

and

$$b = \frac{3\pi\eta D}{k_m}$$

In the present development, V_g, the gas velocity, has been assumed constant. This is, of course, not strictly true, since the presence of the particles (and the viscous effects at the tube wall) act to change the gas velocity, as well as the shock-wave velocity, as the shock progresses down the tube. The phenomena involved, however, do not all act to change the gas velocity in the same direction and have only a small effect for the quantities of material injected into the size tube considered here. The mass effect of the particles is to speed up the gas at distances further from the shock (refs. 4 and 5) (similar to the wall effect in ref. 6), whereas the effect of the volume of the particles is in the other direction (i. e., to slow down the gas behind the shock). In an experiment, more material injected into a smaller tube could produce a noticeable effect, but calculations made for the particle masses considered herein indicated mass and volume loadings to be sufficiently low to have a small effect on the gas velocity, hence V_g is assumed constant. Thus, integration of equation (3) yields

$$V_p = V_g + (V_{p,1} - V_g)e^{-K(t-t_1)} \tag{4}$$

where subscript 1 here refers to initial conditions on arrival of the shock front at the injection point, X_1. Integration of equation (4) yields the particle path equation

$$X_p = X_1 + V_g(t - t_1) + \frac{(V_{p,1} - V_g)}{K}\left[1 - e^{-K(t-t_1)}\right] \tag{5}$$

If the particle is at rest when the shock front arrives, and if t_1 and X_1 are set equal to zero, equations (4) and (5) reduce to

$$V_p = V_g(1 - e^{-Kt}) \tag{6}$$

$$X_p = V_g t - \frac{V_g}{K}(1 - e^{-Kt}) \tag{7}$$

Equations (6) and (7) were used to calculate the velocities of various particles with different values of K (K varies for different types and sizes of particles and with the viscosity of the accelerating gas) while they remained in the slug of shocked hot gas. Particles that are not as yet up to gas speed on the arrival of the contact surface (hot-gas flow duration was calculated by the methods of ref. 7) pass through the contact surface and are still accelerated, but at a slower rate, by the cold, expanded driver gas.

After the contact surface reaches the particle, equations (4) and (5) were used to calculate the trajectory during acceleration by the driver gas. Since the gas conditions (η and k_m) have changed, a new value of K is calculated, X_1 now becomes X_c, $V_{p,1}$ equals the velocity of the particle at the contact surface, and t_1 here is the time at which a particle meets the contact surface. The position downstream of the injection point at which a particle meets the contact surface is obtained by equating the distance the contact surface has traveled from the injection station

$$X_c = V_g(t - \tau) \tag{8}$$

with the distance the particle has traveled (eq. (7)). It was assumed that the injection point of the particles is far enough downstream of the diaphragm so that the shock-tube flow depicted in figure 1 (p. 3) has been established.

Heating of Particle

The driven gas (air) behind a strong shock has been elevated to high temperatures. For the conditions considered in this report, real gas effects were included to calculate the temperatures that ranged from 2970° to $10\,875^{\circ}$ K (ref. 8). This hot gas, used to accelerate particles, can also heat the particles to sufficiently high temperatures to make their trajectories visible on film. To use a photographic method for determining particle velocities, it was therefore necessary to determine the temperature history of the particle. The temperature of an accelerating particle in the hot gas at a time t is obtained by solving the convection equation:

$$-VC_p\rho\frac{dT}{dt} = Ah(T - T_g) \tag{9}$$

Equation (9) is solved in appendix B for the assumption that the specific heat is constant over the temperature range of interest and that $hD/k = 1$ for a sphere with a Reynolds number less than 10 (ref. 9). The solution is

$$T_{p,1} = T_g + (T_r - T_g)e^{-t/C_1} \tag{10}$$

The film chosen for this experiment was a high-speed panchromatic film with a 1250 ASA rating.

The minimum energy density needed for reasonable exposures using this film is 76×10^{-4} erg per square centimeter (ref. 10). To determine the particle temperature necessary to attain this energy density, the radiation law equation was solved in appendix B, with the following result:

$$\left(T_{p,2}\right)^4 = \frac{ER^2V_p(t)}{(2.5)^2\sigma r_\ell^2 D} \tag{11}$$

The time at which the temperature of the particle in the hot stream $T_{p,1}$ reaches the temperature required to expose the film $T_{p,2}$ was calculated from equations (10) and (11). This time was then put into the position equation (7) to give the minimum position downstream of the injection point at which a particle radiates enough energy to be recorded.

If the gas temperature T_g is greater than the sublimation temperature of a particle, any particle that remains in the hot gas long enough will reach its sublimation point. The time t_s at which this takes place is obtained by solving equation (10) for the time at which $T_{p,1}$ equals the sublimation temperature T_s:

$$t_s = C_1 \ln\left(\frac{T_r - T_g}{T_s - T_g}\right) \tag{12}$$

Equation (7), with $t = t_s$ gives the position downstream of the injection point at which sublimation begins.

Once a particle reaches the sublimation point, it continues to sublime until it is gone, if it does not pass behind the contact surface into the cold driver gas. The time at which a particle sublimes to zero radius can be obtained by solving the following heat-balance equation

$$Ah(T_g - T_s) = -\rho H_s 4\pi r^2 \frac{dr}{dt} \tag{13}$$

and solving for t

$$t_{s \to o} = \frac{2\rho H_s r^2}{k(T_g - T_s)} \tag{14}$$

Such a calculation was made in the cases for which it was necessary. The various conditions (initial pressures and gases) for which calculations were made were chosen to be a starting point in picking optimum conditions to accelerate particles in a shock tube. Since a goal in these experiments is the precise knowledge of particle size, the sublimation region should be avoided. The complication of evaluating the reduction in size of the particles due to sublimation was therefore not considered in the present calculations. Such a reduction can be included, if desired, by solving equation (13) for the radius of the particle and substituting r into equations (6) and (7) to calculate the true trajectory of the subliming particle.

Regimes for Particle Acceleration

In most shock tubes, a limitation is imposed by the upper value to which the driver chamber can be pressurized or the temperature to which the driver gas can be raised. In the analytical study to determine conditions in the shock tube under which useful acceleration of small particles could be made, three different driver gas conditions were considered. The first two driver conditions require helium or hydrogen at room temperature, and the third requires electrically heated helium (to give a shock Mach number of 30). With driver chamber conditions thus fixed, the maximum shock Mach number strongly depends on minimum pressure obtainable in the low pressure chamber. However, the actual duration of uniform flow of shocked gas also depends critically on downstream pressures, decreasing as the pressure is decreased. (Duration of uniform flow also decreases with increasing Mach number.) With the preceding considerations in mind, different initial low-pressure side pressures were chosen for the calculations to give a range of shock Mach numbers from 6.5 to 30. A variety of particles was considered for injection into and acceleration by the shocked gas flow. Equations (4) to (7) were used to calculate curves for velocity as a function of position downstream of injection. These are presented as the solid curves in figure 2 for silicon carbide (figs. 2(a) to (e)), tungsten (figs. 2(f) and (g)), and graphite (figs. 2(h) and (i)) particles to show the

character of the problem of accelerating such particles in these short-duration flows. Shown as dot-dashed curves superimposed over these curves are the boundary curves for the points beyond which the various particles are visible (as calculated from eqs. (7). (10), and (11)). The dashed curve superimposed in each of these figures is the locus of positions at which the various particles meet the contact surface (eq. (8)). The locations at which the particles first begin to sublime, are joined by a dash-dash-dot-dot curve indicating the boundary beyond which the particle size would vary from its original value (eqs. (7) and (12)).

For the silicon carbide particles ranging from 2 to 20 microns and accelerated by gas behind a shock of M = 6.5 (fig. 2(a)), only the smaller particles ($<10\mu$) become visible and are accelerated to near gas speed (horizontal dashed line in the figure) before reaching the cutoff point (in these figures, this point is 10 ft downstream of injection). The 14- and 20-micron particles pass behind the contact surface before becoming visible, and hence never become visible during acceleration by the cold expanded driver gas. The uniform shocked-gas flow duration for this case was 375 microseconds. A 2-micron particle starts to sublime at 0.557 foot, and larger particles would start to sublime further downstream (5-μ particle at 4.08 ft). Thus, in this figure, the sublimation curve collapses onto the particle velocity curves near gas velocity and is not shown.

In figure 2(b), the shock Mach number has been increased to 8.38 by reducing the downstream pressure. This, as mentioned previously, causes the flow duration to decrease, in this case to 142 microseconds. The effect immediately apparent is the reduction in the range of size of particles ($<5\mu$), which can be accelerated to near gas speed in the cutoff distance.

In figure 2(c), the initial pressure downstream is reduced to 1 millimeter of mercury, thereby reducing the accelerating flow duration to 98 microseconds while only increasing the shock Mach number slightly. The reduction in flow duration reduces further the size of particle that can be accelerated to near gas speed by the cutoff distance. Here there is no advantage to be gained in decreasing the downstream pressure, since shock-tube pressure-ratio limitations on Mach number are being reached and the only effect is reduction in flow duration.

If a driver gas of lower molecular weight is used, with no change in downstream pressure, a higher shock Mach number is attainable. In figure 2(d) the driver gas is hydrogen, and a gas speed of 13 000 feet per second is obtained. The higher accelerating gas temperatures associated with the increased Mach number cause the gas to have higher viscosity and hence provide higher drag. However, earlier sublimation due to the higher temperatures limits the minimum size particle that can be used, and the shorter flow duration (43μsec) at the higher Mach number limits the maximum particle size. Clearly, the range of size of particles, which can be usefully accelerated by the shocked gas is diminishing, and there appears to be a near upper Mach number limit for accelerating

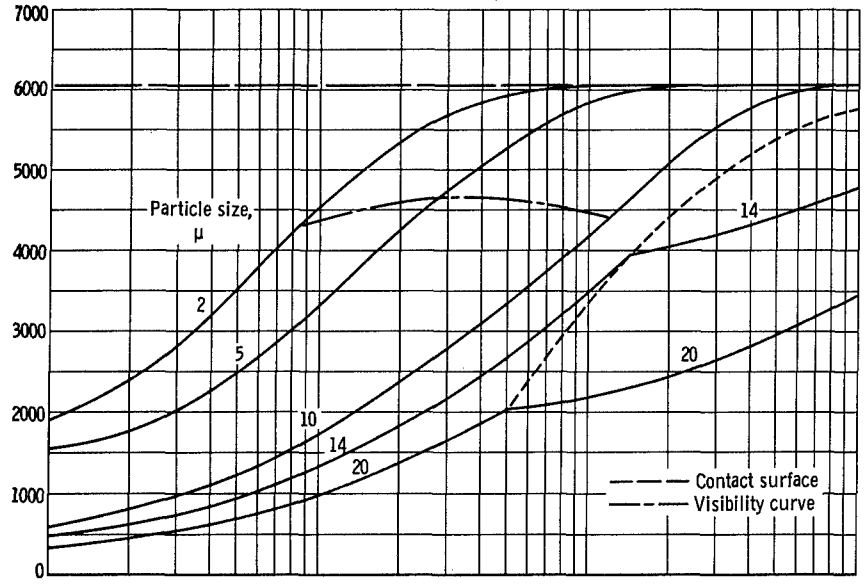

(a) Silicon carbide particles inserted 20 feet from diaphragm. Driver gas, helium at 1000 pounds per square inch pressure; driven gas, air; initial driven gas pressure, 6.7 millimeters of mercury; Mach number, 6.5; gas velocity, 6050 feet per second; gas temperature in region 2, 3000° K; flow duration, 375 microseconds.

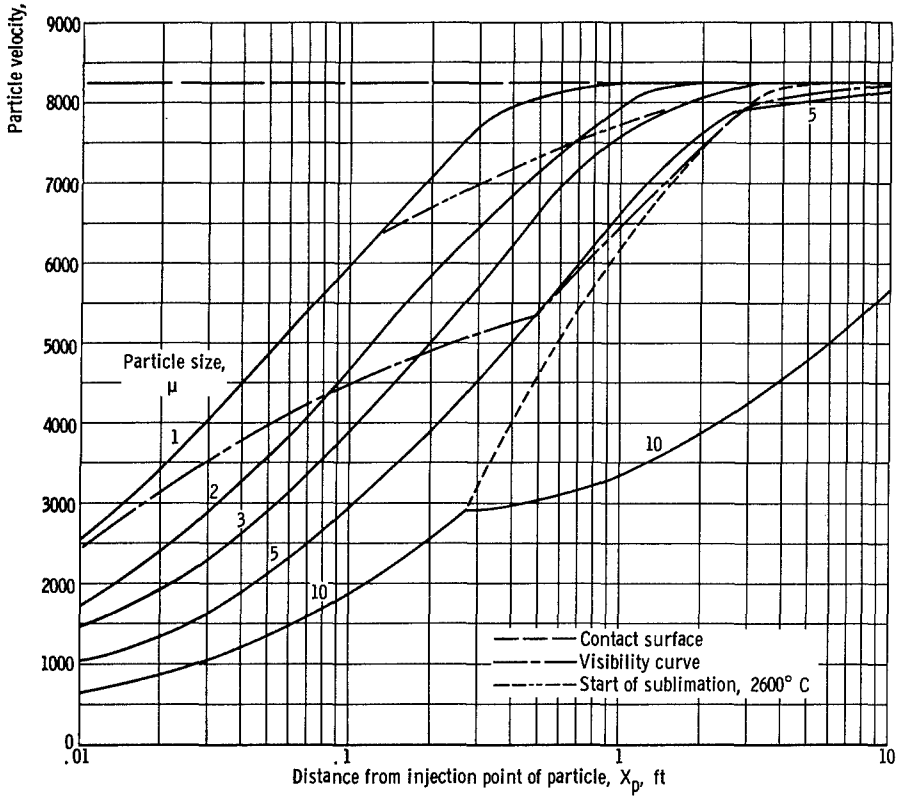

(b) Silicon carbide particles inserted 20 feet from diaphragm. Driver gas, helium at 1000 pounds per square inch pressure; driven gas, air; initial driven gas pressure, 2.0 millimeters of mercury; Mach number, 8.38; gas velocity, 8250 feet per second; gas temperature in region 2, 2970° K; flow duration, 142 microseconds.

Figure 2. - Particle velocity against distance downstream from injection point.

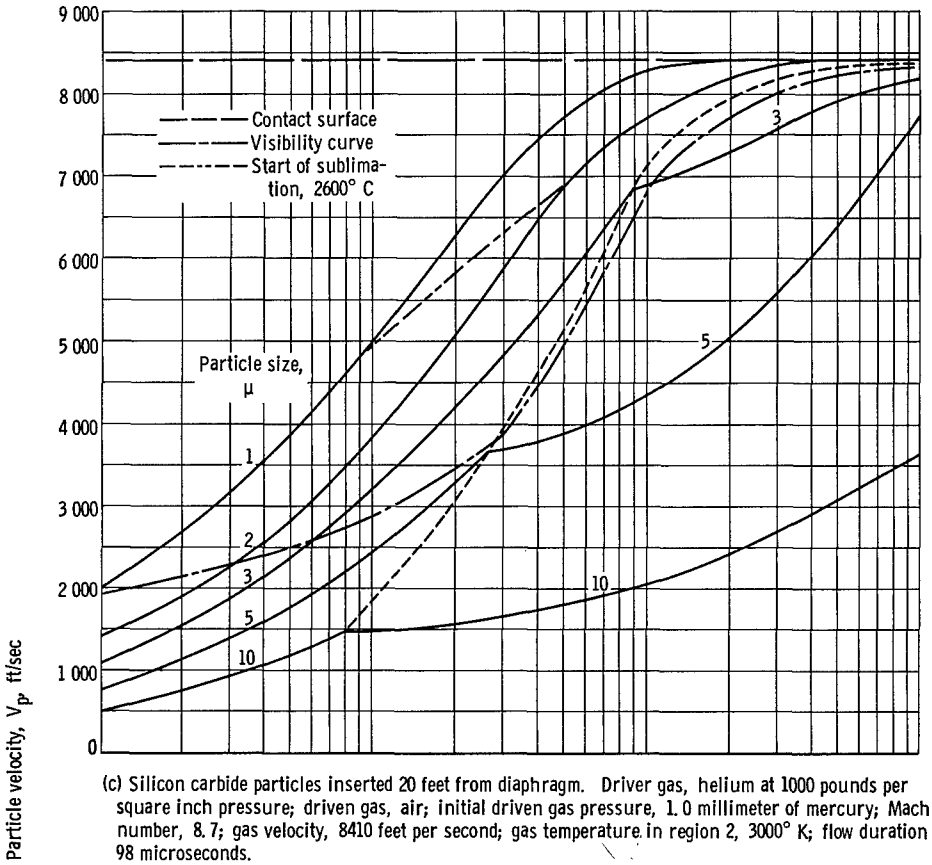

(c) Silicon carbide particles inserted 20 feet from diaphragm. Driver gas, helium at 1000 pounds per square inch pressure; driven gas, air; initial driven gas pressure, 1.0 millimeter of mercury; Mach number, 8.7; gas velocity, 8410 feet per second; gas temperature in region 2, 3000° K; flow duration 98 microseconds.

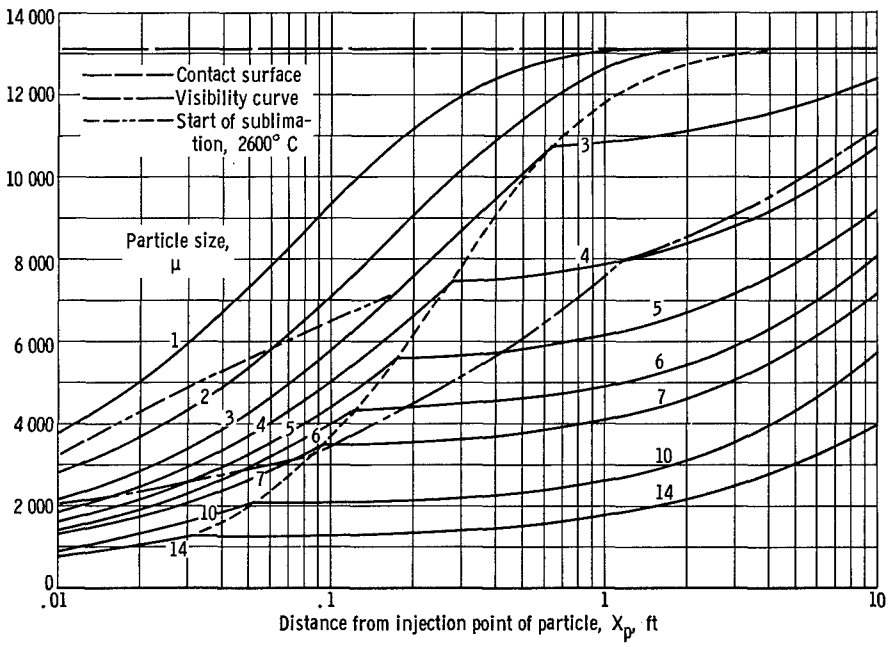

(d) Silicon carbide particles inserted 20 feet from diaphragm. Driver gas, hydrogen at 1500 pounds per square inch pressure; driven gas, air; initial driven gas pressure, 1.0 millimeter of mercury; Mach number, 13.3; gas velocity, 13 100 feet per second; gas temperature in region 2, 4890° K; flow duration, 43 microseconds.

Figure 2. - Continued.

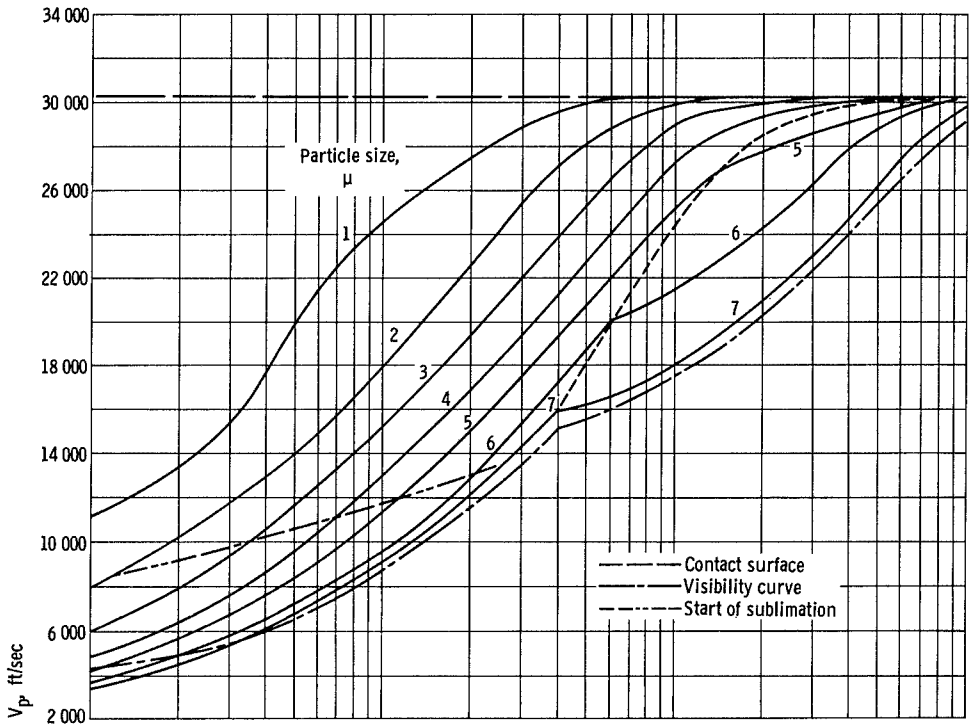

(e) Silicon carbide particles inserted 60 feet from diaphragm. Driver gas, helium at 4000 pounds per square inch pressure electrically heated to 16 900° K; driven gas, air; initial driven gas pressure, 1.0 millimeter of mercury; Mach number, 30; gas velocity, 30 250 feet per second; gas temperature in region 2, 10 875° K; flow duration, 31 microseconds.

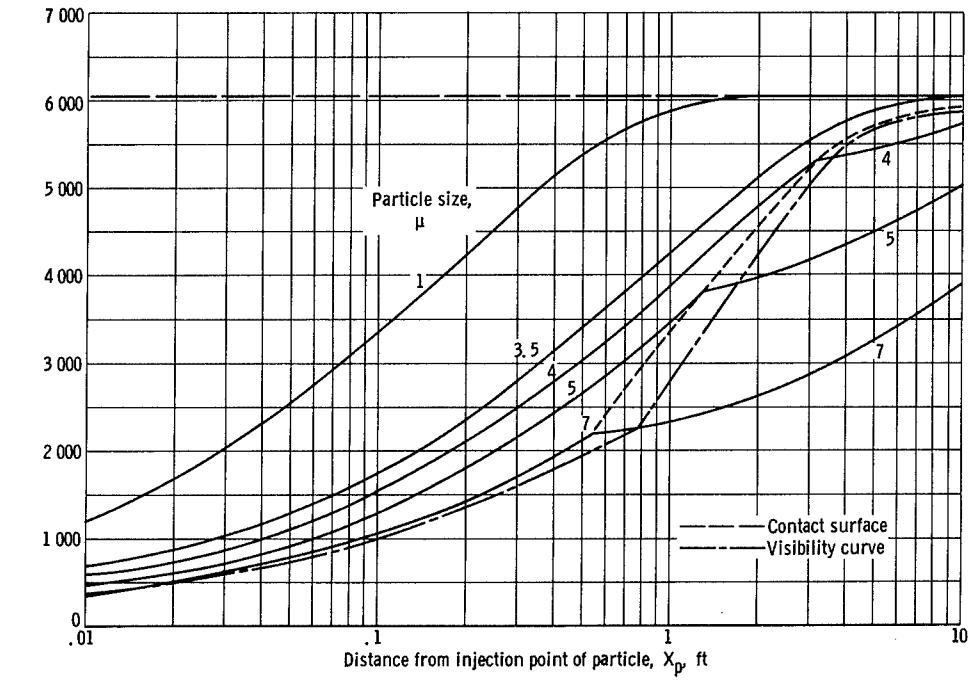

(f) Tungsten particles inserted 20 feet from diaphragm. Driver gas, helium at 1000 pounds per square inch pressure; driven gas, air; initial driven gas pressure, 6.7 millimeters of mercury; Mach number, 6.5; gas velocity, 6050 feet per second; gas temperature in region 2, 3000° K; flow duration, 375 microseconds.

Figure 2. - Continued.

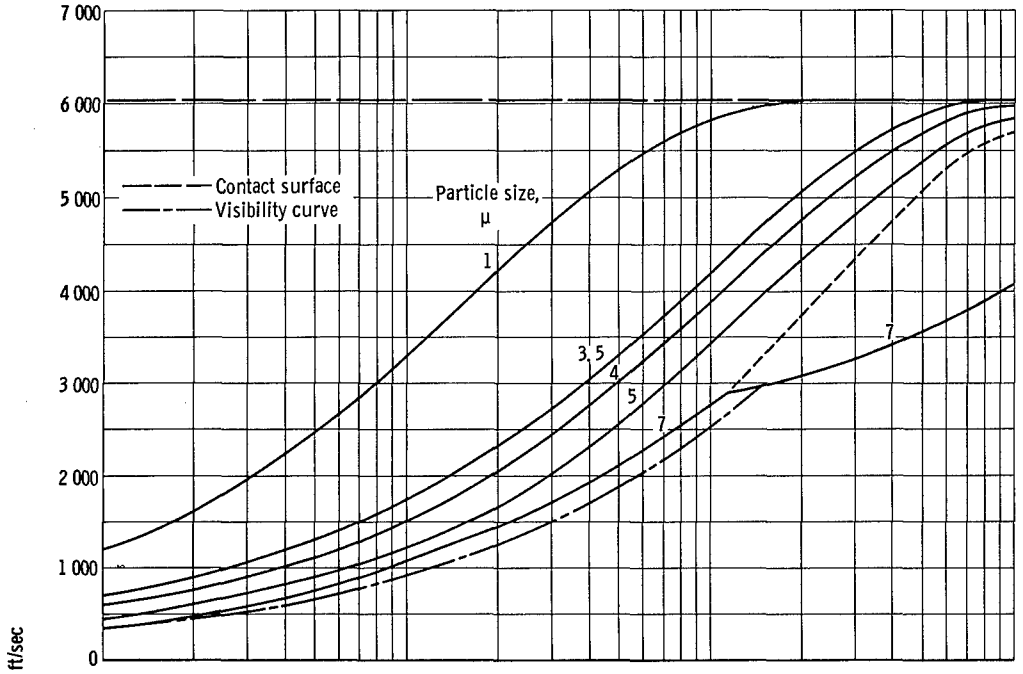

(g) Tungsten particles inserted 30 feet from diaphragm. Driver gas, helium at 1000 pounds per square inch pressure; driven gas, air; initial driven gas pressure, 6.7 millimeters of mercury; Mach number, 6.5; gas velocity, 6050 feet per second; gas temperature in region 2, 3000° K; flow duration, 507 microseconds.

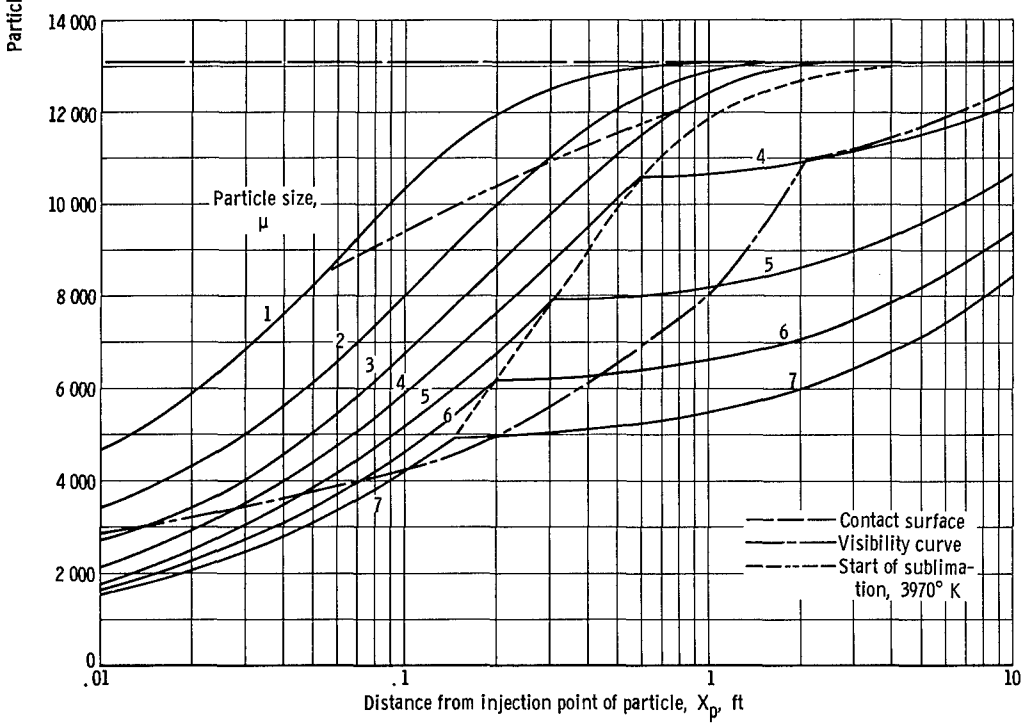

(h) Graphite particles inserted 20 feet from diaphragm. Driver gas, hydrogen at 1500 pounds per square inch pressure; driven gas, air; initial driven gas pressure, 1.0 millimeter of mercury; Mach number, 13.3; gas velocity, 13 100 feet per second; gas temperature in region 2, 4890° K; flow duration, 43 microseconds.

Figure 2. - Continued.

particles of a given material with shock-tube flows. However, in attempting to obtain even higher shock Mach numbers, shock-tube pressure-ratio limitations are overcome by heating the driver gas (ref. 11). This heating (to 16 900° K as in fig. 2(e)) not only increases the Mach number of the shock, but also increases the effectiveness of the expanded driver gas behind the contact surface. As shown in figure 2(e), this driver gas (which is at 2050° K after expansion) quite effectively accelerates a range of particle sizes after the particles have passed through the contact surface. Particles 5, 6, and 7 microns in diameter remain visible and are accelerated to near gas speeds before reaching the cutoff point at 10 feet. This increase in effectiveness is a result of the increased viscosity of the heated driver gas even after expansion. Thus, the apparent limitation on accelerating particles to higher speeds in shock-tube flows may be overcome by heating the driver gas.

Further calculations were made for tungsten particles, to see whether material properties could be used for avoiding the sublimation limitations previously obtained. Figure 2(f) shows that, because of the higher sublimation temperature of tungsten, no sublimation occurs, but the larger density imposes serious limitations on the maximum size of particle that can be accelerated to near gas speed. Injecting particles further downstream increases the hot-gas flow duration, and in figure 2(g), the curves for tungsten particles injected 30 feet downstream of the diaphragm show that the maximum size of particles usefully accelerated does increase. However, inserting particles further downstream in a given length tube automatically reduces the length of tube remaining after injection. Hence, this mechanism for increasing acceleration time is not necessarily advantageous.

To give maximum range in size of particles that can be accelerated to near gas speed, the particle material selected should have a high sublimation point and a low density. These criteria are borne out by the calculations presented in figures 2(a) to (g). To make the particles visible for speed measurements, however, specific heat is an additional characteristic that must be considered.

In figure 2(h), curves for carbon (graphite) particles show that material with a relatively high sublimation temperature and a relatively low density is still not ideal because of relatively low specific heat. Although such particles become visible rapidly, they become invisible rapidly after passing behind the contact surface. Thus choice of materials eases but does not, in general, remove the problems encountered.

Heating of the driver gas appears then to be the most effective means of removing limitations on microparticle acceleration in shock-tube flows. This conclusion is further ther strengthened by the calculations for carbon particles shown in figure 2(i), in which the heated helium driver gas successfully accelerates 6- and 7-micron-diameter graphite particles to 30 250 feet per second while keeping the particles visible and avoiding the problems of sublimation.

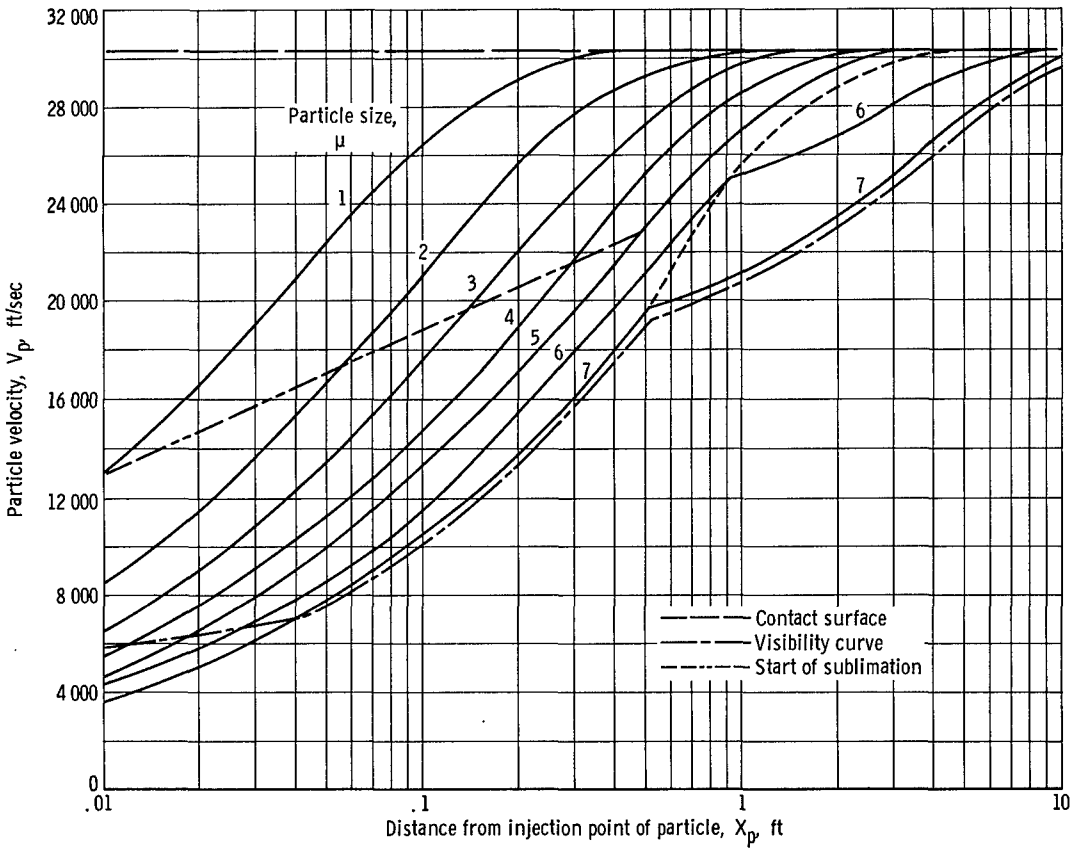

(i) Graphite particles inserted 40 feet from diaphragm. Driver gas, helium at 4000 pounds per square inch pressure electrically heated to 16 900° K; driven gas, air; initial driven gas pressure, 1.0 millimeter of mercury; Mach number, 30; gas velocity, 30 250 feet per second; gas temperature in region 2, 10 875° K; flow duration, 27 microseconds.

Figure 2. - Concluded.

The preceding calculations were made by using the Stokes drag law, although this is conservative, to show the character of the problems involved when accelerating microparticles in shock-tube flows. Actual drag coefficients may be as much as an order of magnitude larger than the Stokes value (refs. 12 and 13). This would not change any conclusions drawn from the material presented in figure 2. It would only have the effect of making the curves shown valid for slightly larger particles.

LABORATORY EXPOSURE OF REFLECTIVE SURFACES

The short-duration flows in a 2.9-inch-diameter shock tube (shown in fig. 3(a)) with a driven section 35 feet long (fig. 3(b)) were used to accelerate micron-size particles in the experimental portion of the program. Helium at 1000 pounds per square inch was used as the driver gas, and air was the driven gas in the low-pressure section into which the shock was fired. A copper diaphragm separating the chambers was ruptured by an

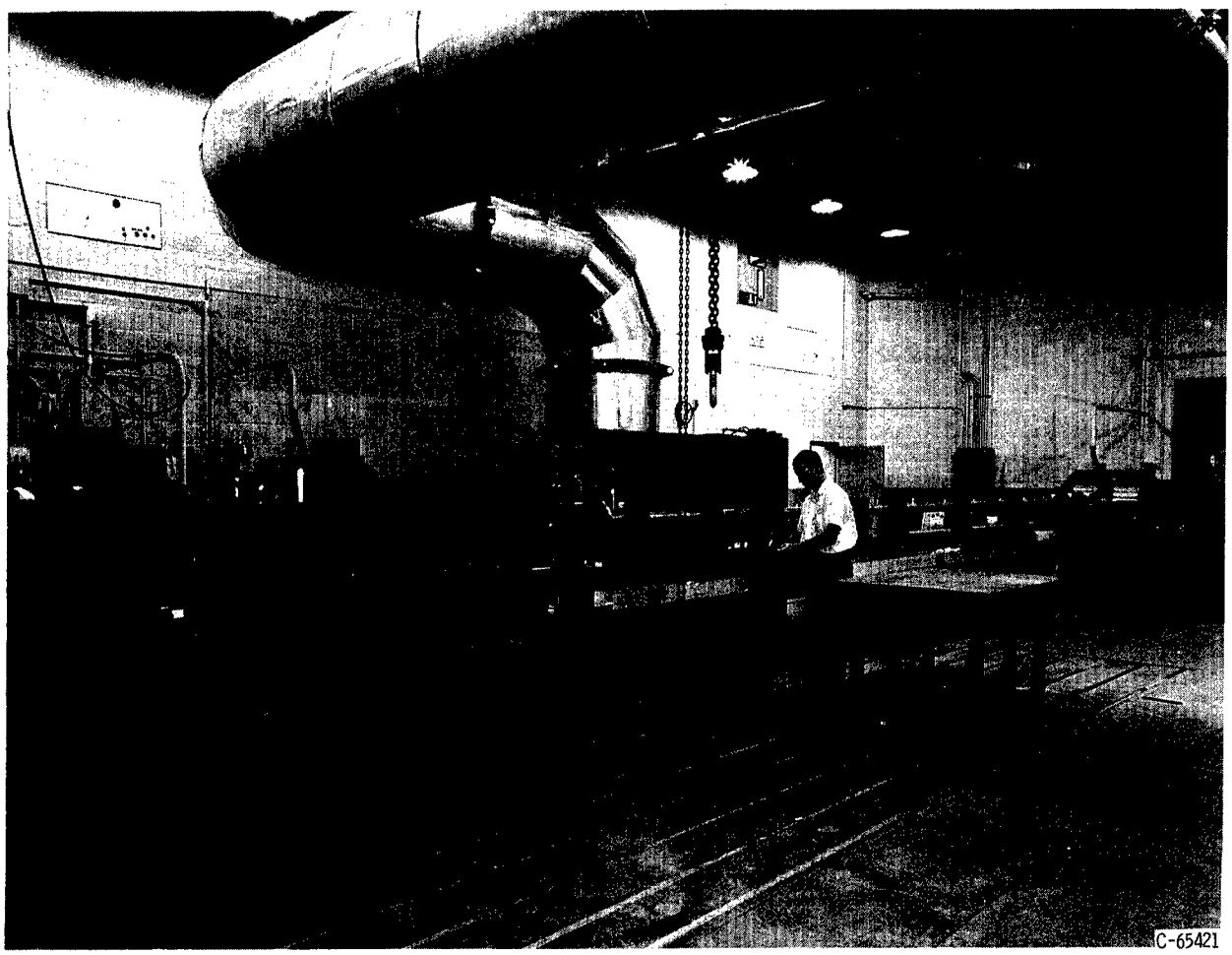

(a) Overall view.

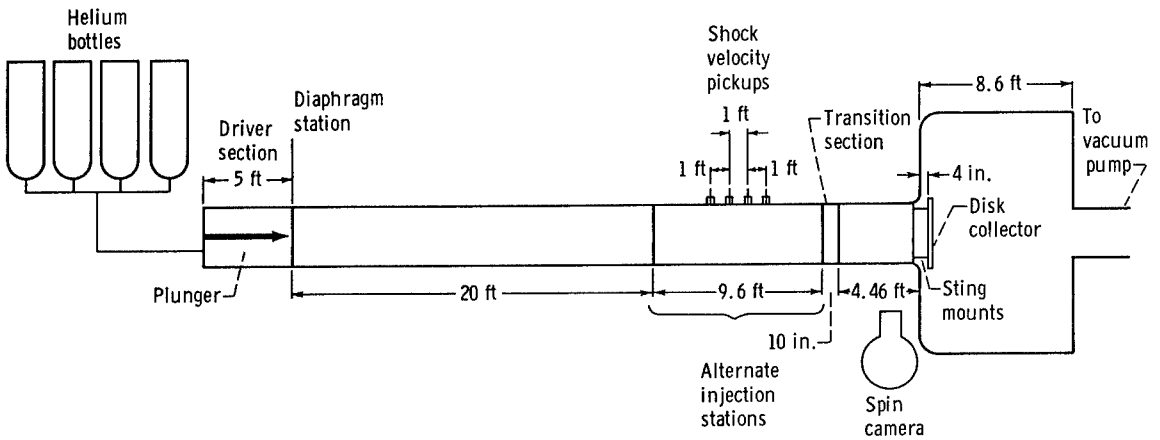

(b) Schematic drawing indicating position of shock velocity pickups and camera location.

Figure 3. - 2.9-Inch-diameter shock tube.

arrowhead plunger. This system was very successful in initiating shocked flows while preventing any diaphragm particles from tearing loose and interfering with the experiment.

The driven end of the 2.9-inch shock tube consisted of two tube sections in series, 20 feet long and 9.6 feet long, respectively. These were followed by a transition section 10 inches long and a rectangular test section 4.46 feet long which emptied into an 18-inch-diameter dump tank 8.6 feet long. Shock-speed measurements were made with thin-film platinum gages on the wall of the driven tube just upstream of the transition section. Particle velocity measurements were made by streak film photography of the glowing particles in the test section. The particle collection station was just downstream of the test section in the dump tank. Test surfaces placed at the collection station were exposed to impaction by a known mass of particles arriving at measured speeds. For actual exposures of surfaces, only particles that would be accelerated to gas speeds were used in the experiment. This exposure was correlated with the change of test surface properties as measured by optical instruments. The optical measurements made were of test surface reflectance before and after exposure and involved the use of a spectral reflectometer in conjunction with a heated cavity (hohlraum) blackbody radiator.

Particle Injection

Particles to be injected into the stream were placed on the horizontal surface of a sharp-edged thin plate located at the injection station in the center of the tube cross section. It was from this surface that the particles were picked up by the high-speed flows following passage of the shock. The data presented herein were obtained for silicon carbide particles injected at a point 20 feet downstream of the diaphragm. The injection system required great care but with this care quite repeatable particle measurements of collector weights and distribution of particles were possible.

Velocity Measurements

Velocity measurements of the gas-heated, radiating cloud of particles were made by recording particle trajectories with a streak camera on 1250 ASA film. The camera, which had a depth of field of 1/8 inch, was focused on the center vertical plane in the test section of the shock tube (see fig. 3(b)). This plane is parallel to the longitudinal axis of the tube and therefore, of course, also parallel to the flow direction. The vertical sides of the rectangular test section of the shock tube are provided with windows that allow observation of the flow of particles. A slit $2\frac{5}{8}$ inches long and $\frac{5}{8}$ inch high was mounted on

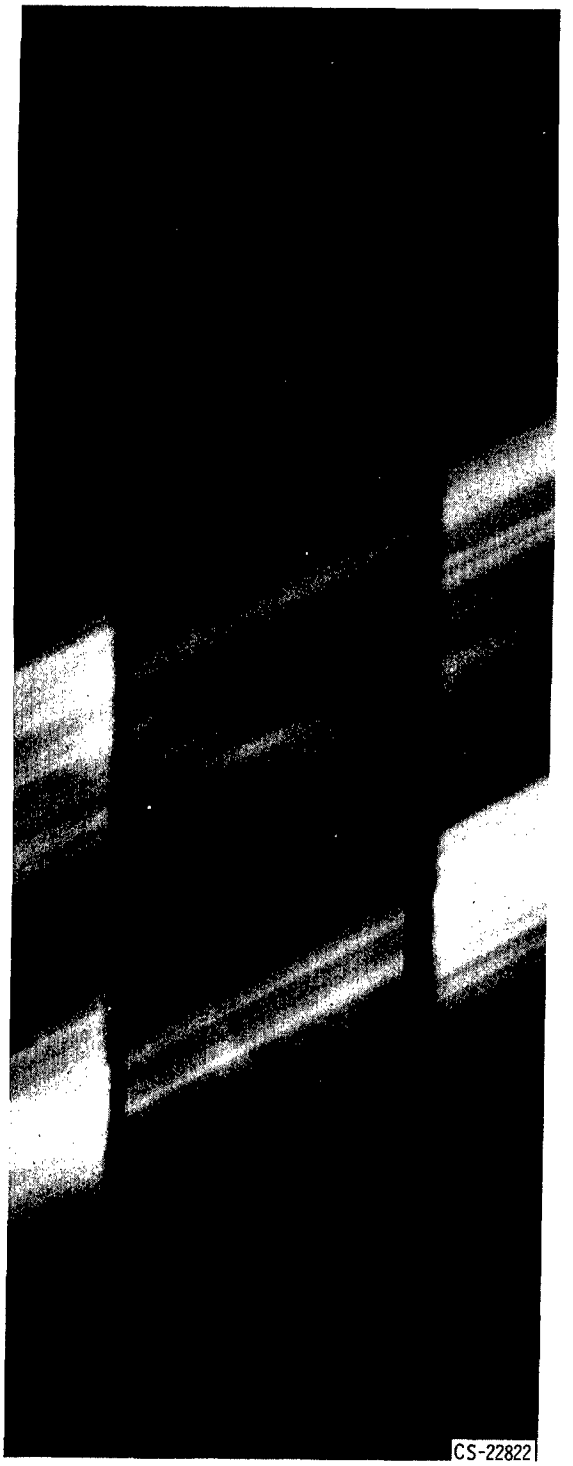

Figure 4. - Streaks made by radiation given off by 2- to 14-micron-diameter silicon carbide particles at Mach number 6.5 taken 4.45 feet downstream of injection station.

the front of one of the glass windows. A typical photograph is shown in figure 4. In this case, the streaks were made by radiation from silicon carbide particles 2 to 14 microns in diameter. The shock Mach number was 6.5, and the initial pressure P_1 was 6.7 millimeters of mercury. The velocity is determined from the angle a streak on the film makes with the horizontal. The speed of the film (the time axis) is accurately known (to a small fraction of a percent) from precise measurements of the rotational speed of the mirror, which beams the picture to the film at the focal cylinder in the camera (mirror rotational speeds are 240 to 500 rps). Thus, particle speeds can be measured with good accuracy. To make certain that the streaks used for velocity measurements were made by particles and not by glowing gas, runs were made for which no particles were injected into the stream and the film exposed in the usual way. Invariably, after such runs the film appeared unexposed, indicating that particles were necessary to obtain the streaks on the film, and that, therefore, the streaks were indeed made by radiating particles. Velocity measurements were also successfully made for aluminum oxide, nickel and carbon, as well as for glass microballoon particles, although these were not used for surface exposures in the present study.

No attempt was made to measure the velocity of a single particle by using the streak camera technique, since the development of the technology required to inject and locate a single particle would multiply the difficulties of the experiment many times. Cases for actual exposures of surfaces were

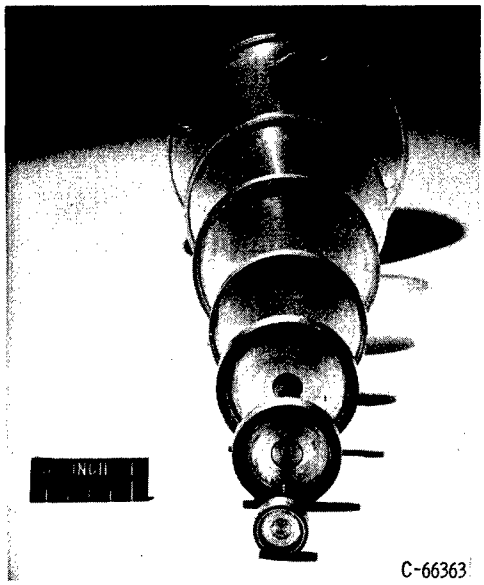

C-66363

Figure 5. - Disk collectors of various sizes (1/2 to $3\frac{13}{16}$ in. in diam) used to make integrated density measurements.

limited to those for which all particles involved would be near gas speed. Since the original purpose of using the shock tube was to accelerate micron-size particles for surface erosion studies, and such erosion requires exposure to impact by many particles, experiments with a single particle were not required.

Distribution of Particles at Impact

To determine the distribution of the particles over the plane at the end of the shock tube, measurements were made by collecting silicon carbide particles on various diameter disk collectors, shown in figure 5. The collectors range in diameter from $\frac{1}{2}$ to $3\frac{13}{16}$ inches and were coated with vacuum grease to ensure capture of the accelerated particles. The largest diameter disk ($3\frac{13}{16}$ in.) was held in the tube by sting mounts and placed in the dump tank 4 inches from the end of the test section (see fig. 3(b), p. 16). It was presumed, and later verified, that all the particles actually accelerated would be collected by this disk. The smaller size disks were placed in the shock tube by mounting them on a $3\frac{13}{16}$-inch-diameter plate that was sting mounted in the shock tube in the same manner and at the same station as the $3\frac{13}{16}$-inch collector disk. The coated disk collectors were weighed on an analytical balance before and after bombardment by particles. The difference in weight gives the mass of particles collected by each disk, and over the range of collector disk size, the radial density distribution. When no particles were injected, as accurately as could be measured (50 μg) the weight of the collectors was unchanged. The mass of the silicon carbide particles collected, normalized to the mass of particles collected on the largest size disk (i.e., to the total amount actually accelerated down the tube) is plotted against the diameter of the disk collectors in figure 6. It can be seen that the radial distribution of particles varied slightly with the Mach number for those shown and was essentially independent of the total initial mass of particles placed in the shock tube over the range of mass increments used in this experiment. For any intermediate size disk, the mass of silicon carbide particles falling on the disk could be quite satisfactorily repeated to within a few percent. Collections attempted for other projectile materials and particle-size range indicated that such accurate collections as with silicon carbide (of 6-μ average diameter) could not always be accomplished by the technique described. Some of the other types of particles successfully accelerated tended to agglomerate before insertion

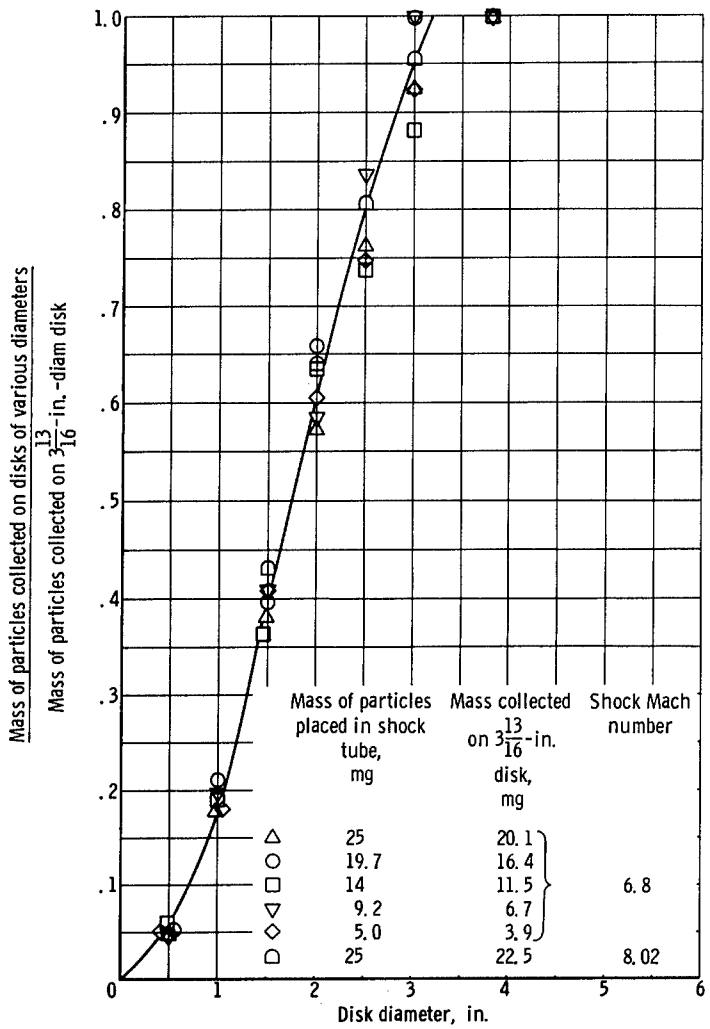

Figure 6. - Mass of particles collected on disks of various diameters normalized to total mass collected as function of diameter of disk collector.

in the shock tube as a result of collected moisture or static charge. These agglomerates removed large amounts of the vacuum grease coating the disk collectors and thus made weight measurements with this type of collector unfeasible. For quantitative exposures, an arbitrary minimum of 75 percent was set for the percentage of the total mass injected to be collected on the largest ($3\frac{13}{16}$ in.) disk.

This minimum figure was set in order to include the possibility that some of the measurement decrement be a result of loss of collector mass and in this way limit the maximum error that might arise. Since collection measurements were repeatable to ±5 percent and more than 80 percent of the total mass injected was usually collected, this total amount collected was considered to be the amount actually accelerated. No total collection weight measurements ever exceeded the weight of projectile material placed in the tube.

If this minimum was not met for a given projectile material and size, no quantitative exposures were made. The only projectile particles used for quantitative surface exposure in the present report (SiC, 2 to 14 μ) met this requirement. More than 75 percent of those placed at the injection station were collected on the largest disk. The normalization in figure 6 is based on the assumption that the total mass actually accelerated will be collected on the $3\frac{13}{16}$-inch-diameter disk. The assumption appears to be true since the 3-inch-diameter disk collects almost the same amount (~95 percent) as does the larger disk. The abrupt leveling off of the curve at 3 inches in diameter indicates that further increase in collection disk diameter would not increase the amount collected.

Optical Properties of Impacted Surfaces

If a polished metal surface is hit by a microparticle at hypervelocity, a hemispherical crater is left in the surface. The volume of the crater depends on the target material and has been shown to vary directly with the kinetic energy of the projectile (in the range of speeds considered here, ref. 14). The area of the surface damaged depends, of course, on the crater volume. The resulting total reflectance of a surface can be described in terms of a replacement, over the area of damage, of the original reflectance $\overline{\rho}_i$ with a new reflectance $\overline{\rho}_\infty$. This can be stated mathematically as

$$\rho_f\left\{A_D(\epsilon)\right\} = \frac{\overline{\rho}_i}{A_o}\left[A_o - A_D(\epsilon)\left(1 - \frac{\overline{\rho}_\infty}{\overline{\rho}_i}\right)\right] \tag{15}$$

With this model, it is clear that further damage to the surface can occur only on the remaining undamaged area. From this it follows that

$$\frac{dA_D}{d\epsilon} = K_1\left[A_o - A_D(\epsilon)\right] \tag{16}$$

Solving equation (16) for $A_D(\epsilon)$ gives

$$A_D(\epsilon) = A_o\left(1 - e^{-K_1\epsilon}\right) \tag{17}$$

Substituting for $A_D(\epsilon)$ from equation (17) into equation (15) yields

$$\bar{\rho}_f(\epsilon) = \bar{\rho}_i \left[1 - \left(1 - \frac{\bar{\rho}_\infty}{\bar{\rho}_i} \right) \left(1 - e^{-K_1 \epsilon} \right) \right] \tag{18}$$

Equation (18) describes the reduction in reflectance of any exposed area A_o that is struck by hypervelocity particles, the sum of whose kinetic energy is ϵ. The constant K_1, which is the fraction of fresh area damaged per unit of exposure energy, can be obtained from equation (16) for the case of zero exposure ($A_D = 0$) as

$$K_1 = \frac{d\left(\frac{A_D}{A_o}\right)}{d\epsilon} \tag{19}$$

For the first increment of exposure (i.e., the first hit), if the crater volume is proportional to particle kinetic energy,

$$\frac{dA_D}{d\epsilon} = \frac{\left(3\pi^{1/2} \frac{m_p V_p^2}{4E_{cr}} \right)^{2/3}}{\frac{m_p V_p^2}{2}} \tag{20}$$

where the denominator $m_p V_p^2/2$ is the single particle kinetic energy, the numerator is the surface area of the first crater, and E_{cr} is the cratering energy density, that is, the projectile kinetic energy required per unit volume of the crater formed in the target. The cratering energy density E_{cr} has been evaluated for many materials and is available in the literature (refs. 14 to 16). Solving equations (19) and (20) for K_1 results in

$$K_1 = \frac{1}{A_o} \left(\frac{3\pi^{1/2}}{2E_{cr}} \right)^{2/3} \left(\frac{m_p V_p^2}{2} \right)^{-1/3} \tag{21}$$

It is clear from equation (21) that the assumption made earlier, that K_1 is constant for a given particle kinetic energy, is essentially the assumption that E_{cr} is constant. Finally, equation (18) becomes

$$\bar{\rho}_f(\epsilon) = \bar{\rho}_i \left(1 - \left(1 - \frac{\bar{\rho}_\infty}{\bar{\rho}_i} \right) \left\{ 1 - e^{-\left[\frac{1}{A_o} \left(\frac{3\pi^{1/2}}{2E_{cr}} \right)^{2/3} \left(\frac{m_p V_p^2}{2} \right)^{-1/3} \epsilon \right]} \right\} \right) \tag{22}$$

Reflectance as a function of exposure can be plotted directly from equation (22) for a given target material, projectile, and projectile kinetic energy. Values for E_{cr} were obtained from reference 16, while $\bar{\rho}_\infty$ was the reflectance determined by exposing a target to impaction by microparticles until no further change in reflectance could be measured. Equation (22) was used for comparison with the reflectance measurements described in the next section.

Measurement of Optical Properties

Test surfaces (for cases described herein, generally polished metals) of disks 15/16 inch in diameter and 1/64 to 1/16 inch thick were exposed to impaction by known amounts of particles of known size and composition at measured speeds. With exposure thus known, it was desirable to determine whether the effects of this exposure on surface optical properties would be reproducible at any given exposure. Infrared reflectance was chosen as an operational parameter, and spectral reflectance measurements of exposed disks were made from 1.5 to 15.5 microns with an infrared spectrometer coupled with a heated-cavity blackbody. In such a system, the spectrometer compares the radiation at a given wavelength from a 600° C blackbody cavity with the total radiation reflected from a water-cooled sample within the cavity. The ratio of the amount reflected to the blackbody value is taken as the reflectance at that wavelength and is designated as $\rho_{h\text{-}a}(\lambda)$.[1] To determine a total (wavelength independent) reflectance, this spectral value is weighted for the radiation from a blackbody at 420° K. Total final reflectance is defined here as

$$\bar{\rho}_f = \frac{\int_{\lambda_1}^{\lambda_2} \rho_{h\text{-}a}(\lambda) I_{BB}(\lambda) d\lambda}{\int_{\lambda_1}^{\lambda_2} I_{BB}(\lambda) d\lambda} \tag{23}$$

for $\lambda_1 = 1.5$ microns and $\lambda_2 = 15.5$ microns. It is this average value that characterizes the optical condition of the surface and is used to determine the effect of exposure.

[1]These data were obtained by E. Anagnostou of Lewis.

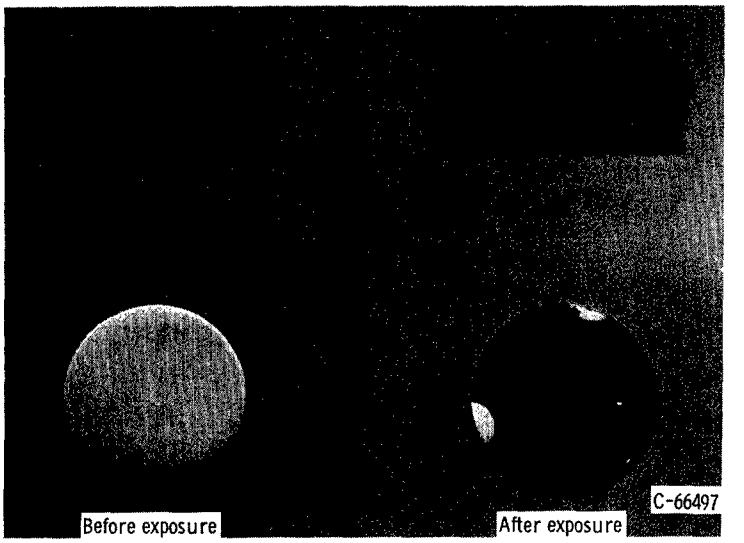

Figure 7. - Sample aluminum disk 15/16 inch in diameter before and after exposure to 2- to 14-micron silicon carbide particle flows.

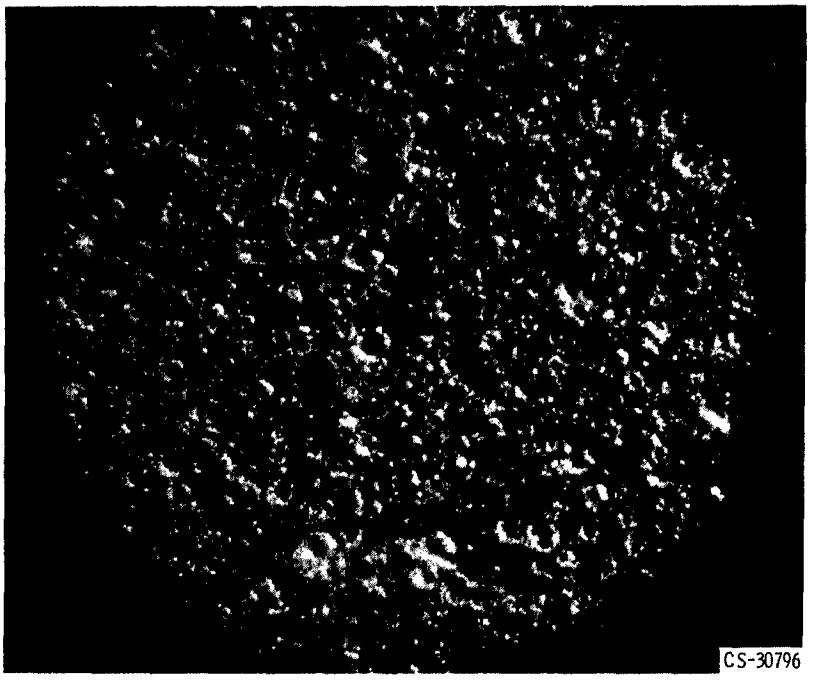

Figure 8. - Photomicrograph of exposed surface shown in figure 7. X500.

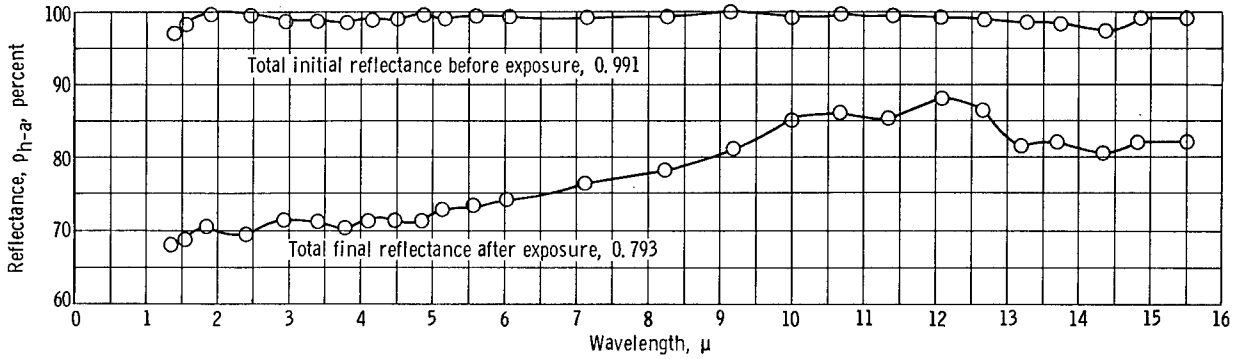

Figure 9. - Spectral reflectance ρ_{h-a} as function of wavelength for polished hard aluminum (2024) disk exposed to 1.21 joules of 6-micron-diameter silicon carbide particles.

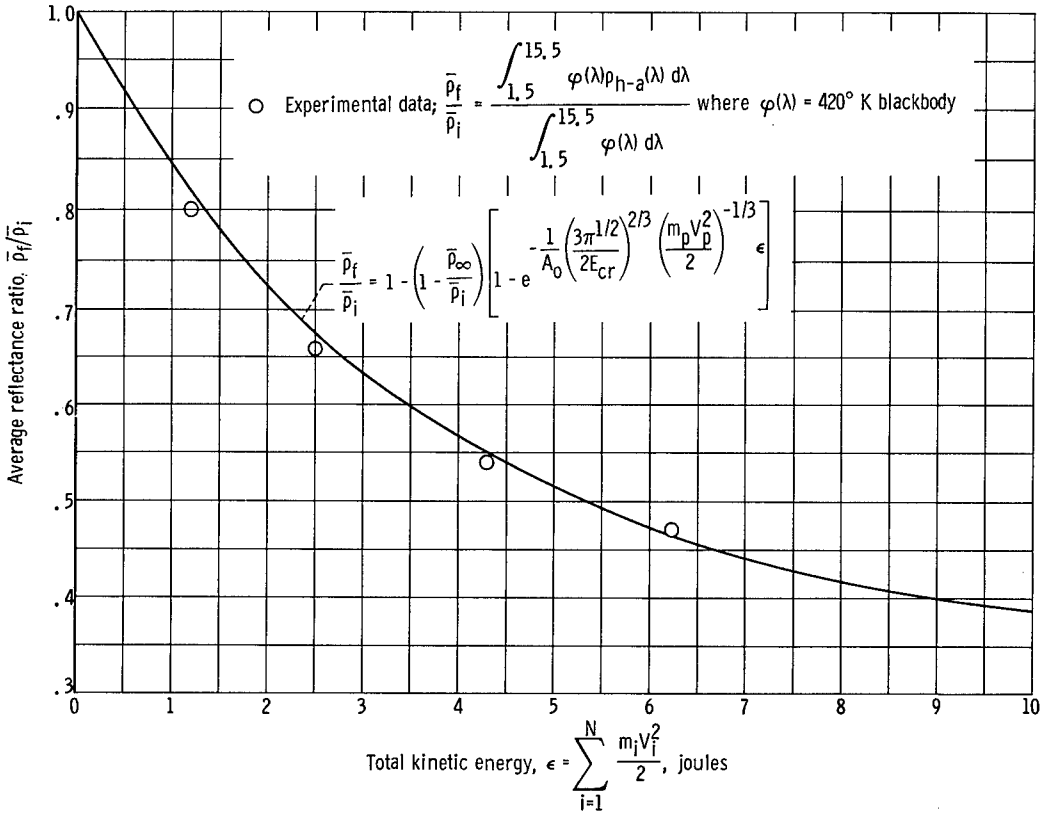

Figure 10. - Plot of reflectance ratio as function of kinetic energy of 6-micron-diameter silicon carbide particles falling on an aluminum disk 15/16 inch in diameter. Total effective reflectance for area damaged by crater, $\bar{\rho}_\infty$, 0.34; total initial reflectance of area A_0 before exposure, $\bar{\rho}_i$, 0.991; disk area, A_0, $\pi r^2 = \pi(15/32 \text{ in.})^2$; cratering energy density, E_{cr}, 1.65×10^{10} erg per cubic centimeter; particle mass, m_p, 3.62×10^{-10} gram; particle velocity, V_p, 8200 feet per second.

Degradation of Reflectance with Exposure

A photograph of a typical aluminum disk before and after exposure to microparticle impact is shown in figure 7. The exposed surface magnified 500 times is shown in figure 8, where the hemispherical character of the craters is evident.

The values of ρ_{h-a} as a function of wavelength for a 15/16-inch-diameter aluminum disk before and after exposure to 1.21 joules of silicon carbide particles is presented in figure 9. Note that the aluminum before exposure has, within the accuracy of the measurement, a reflectance of approximately 1.0 over the range 1.5 to 15.5 microns. Averaging this with equation (23) gives a $\overline{\rho}_i$ of 0.991, and this is shown in the figure. After exposure, the reduction in reflectance is not the same at all wavelengths, and the weighting by means of equation (23) gives a value for $\overline{\rho}_f$ of 0.793. Note that for the shorter wavelengths in the infrared region, which are of greater interest for solar radiation, the effect of degradation of reflectance is the largest.

The measured ratio of $\overline{\rho}_f/\overline{\rho}_i$ for various exposures is presented in figure 10, where the point for 1.21 joules is this ratio for the data presented in figure 9. The solid line is a plot of equation (22) with $\overline{\rho}_\infty$ as measured in the present experiment and E_{cr} from reference 16. The excellent fit may be fortuitous and is not necessarily indicative of the accuracy to be expected in this work. It does indicate, however, that with reasonable values for the material constants, a good estimate can be made of the surface degradation as a result of hypervelocity exposure to microparticles in the laboratory.

CONCLUDING REMARKS

An analysis is presented to establish the feasibility of accelerating microparticles to hypervelocities in shock-tube flows. Conservative assumptions with respect to drag were made because they were simple, and allowed the greatest clarity in the presentation of the character of the problem. Regimes for useful acceleration of microparticles were found indicating that these short-duration flows can accelerate particles over a useful range of sizes to speeds of interest. Experiments showed that sufficiently accurate measurements of speed and quantity of impinging material can be made for characterizing the exposure of target materials. At least for polished metal surfaces, optical properties of the surfaces correlated with the exposure. An analytical determination of the variation in surface reflectance of these targets with exposure compares quite adequately with experimentally determined values. The analysis suggests a means of extending measurements of reflectance degradation in the laboratory to predictions for surfaces under actual meteoroid dust exposure in space. Such an estimate was made in reference 17.

Lewis Research Center,
National Aeronautics and Space Administration,
Cleveland, Ohio, September 29, 1965.

APPENDIX A

SYMBOLS

A	surface area of particle
$A_D(\epsilon)$	damaged area after exposure to ϵ
A_f	area of film exposed by radiating particle, A/F^2
A_o	disk area
b	$3\pi\eta D/k_m$
C_p	specific heat of particle
C_1	$2r^2C_p\rho/3k$
D	particle diameter
E	minimum energy density needed to expose high-speed panchromatic film (1250 ASA)
E_{cr}	cratering energy density
F	demagnification factor, L/L_f
f_d	drag force
H_s	heat of sublimation
h	heat-transfer coefficient
$I_{BB}(\lambda)$	spectral energy distribution of 420° K blackbody
K	$b/m_p = 18\eta/k_m\rho D^2$
K_1	fraction of fresh area damaged per unit of exposure energy, $\frac{1}{A_o}\left(\frac{3\pi^{1/2}}{2E_{cr}}\right)^{2/3}\left(\frac{m_pV_p^2}{2}\right)^{-1/3}$
k	thermal conductivity of accelerating gas
k_m	Cunningham-Millikan correction factor, $1 + \frac{0.16\times10^{-4}\ \text{cm}}{D}\ \frac{T}{T_o}\ \frac{P_o}{P}$
L	length in object plane
L_f	length in focal plane
M_s	Mach number
m_p	particle mass
p	pressure
p_1	initial downstream pressure, mm Hg
p_4	initial driver pressure
R	distance from particle to lens of streak camera
r	particle radius
r_ℓ	radius of camera lens
T	temperature
T_g	gas temperature
$T_{p,1}$	temperature of particle in hot gas
$T_{p,2}$	temperature required for particle traveling at V_p to radiate minimum energy needed to expose film
T_r	room temperature
T_s	particle sublimation temperature

t time

t_s time it takes for particle to reach its sublimation temperature

$t_{s \to 0}$ time for sublimation to zero radius, eq. (14)

t_1 any time after arrival of shock wave

V volume

V_g gas velocity

V_p particle velocity, ft/sec

$V_{p,1}$ velocity of particle at time t_1

X_c position of contact surface

X_p distance from injection point of particle, ft

X_1 position of particle at time t_1

ϵ total kinetic energy of N particles falling on area A_o,

$$\sum_{i=1}^{N} \frac{m_i V_i^2}{2}, \text{ joules}$$

η viscosity

λ wavelength

ρ density of particle

$\overline{\rho}_f$ total final reflectance of area A_o after exposure to ϵ

$\overline{\rho}_i$ total initial reflectance of area A_o before exposure

$\overline{\rho}_\infty$ total effective reflectance for area damaged by crater

$\rho_{h\text{-}a}$ spectral hemispheric angular reflectance

σ Stefan-Boltzmann constant

τ gas flow duration

APPENDIX B

CALCULATION OF TEMPERATURES FOR VISIBILITY ON FILM OF HEATED PARTICLES

Temperature History of Accelerated Particle

The heat-balance equation between the gas and the particle is

$$-VC_p\rho \frac{dT}{dt} = Ah(T - T_g) \tag{9}$$

Over the temperature range involved, an appropriate average C_p was used. With the assumption of spherical particles, equation (9) becomes

$$-\frac{4}{3}\pi r^3 C_p \rho \frac{dT}{dt} = 4\pi r^2 h(T - T_g) \tag{B1}$$

The experimental data of reference 18 for spheres indicated that for $Re \leq 10$, hD/k approached 1, although the theoretical value approaches 2 for $Re \to 0$. Choice of a constant value of 1.0 for hD/k is strengthened by the work of reference 9. Although the heat transfer in reference 9 was done for cylinders, the effect of Mach number is shown in the slip-flow region and indicates that, as the Mach number decreases, the Reynolds number also decreases in such a manner that the Nusselt number stays approximately constant. Thus, if $h = k/D$ is substituted into equation (B1)

$$\frac{-2r^2 C_p \rho}{3k} \frac{dT}{dt} = T - T_g \tag{B2}$$

Letting $C_1 = \frac{2r^2 C_p \rho}{3k}$ results in

$$-\int_{T_r}^{T_{p,1}} \frac{C_1\, dT}{T - T_g} = \int_0^t dt \tag{B3}$$

On integration, equation (B3) becomes

$$T_{p,1} = T_g + (T_r - T_g)e^{-t/C_1} \tag{B4}$$

Minimum Particle Temperature Required to Expose Film

The minimum energy needed to expose high-speed panchromatic film with a 1250 ASA rating is 76×10^{-4} erg per square centimeter. The value was obtained by the manufacturer by using a standard tungsten light source. Now the tungsten source radiates at about the same temperature as the particles in the hot gas (~3000° K). The film used is sensitive between 0.3 to 0.7 micron, and at these wavelengths there is little difference in the spectral matching to the film of radiation given off by the particles and that given off by the calibrating source. Thus the energy density figure given was used unchanged. To determine the temperature needed by the particles to radiate sufficient energy to expose the film, the radiation law is used in the form

$$EA_f = \epsilon\sigma A(T_{p,2})^4\left(\frac{A_{lens}}{4\pi R^2}\right)t \tag{B5}$$

where A_f is the area of the film exposed by the particle radiation. Assuming $\epsilon = 1$, that is, a blackbody, using the known demagnification factor ($F = L/L_f$) of 2.5 from the geometry, and substituting for A_f, A, and A_{lens} give equation (B5) in the form

$$\frac{E(\pi r^2)}{(2.5)^2} = \sigma(4\pi r^2)(T_{p,2})^4\left(\frac{\pi r_\ell^2}{4\pi R^2}\right)t \tag{B6}$$

The time of exposure t was assumed equal to the time it takes for a particle to pass through its diameter D going at a velocity $V_p(t)$:

$$t = \frac{D}{V_p(t)} = \frac{D}{V_g(1 - e^{-kt})} \tag{B7}$$

Substituting equation (B7) into equation (B6) and solving for $(T_{p,2})^4$ yield

$$(T_{p,2})^4 = \frac{ER^2V_p(t)}{(2.5)^2\sigma r_\ell^2 D} = \frac{ER^2V_g(1 - e^{-kt})}{(2.5)^2\sigma r_\ell^2 D} \tag{B8}$$

REFERENCES

1. D'Aiutolo, C. T.: Meteoroid Hazards in Near Earth and Deep Space. Paper Presented at Manned Planetary Mission Tech. Conf., Lewis Research Center, Cleveland (Ohio), May 21-23, 1963.

2. Alexander, W. M.; McCracken, C. W.; Secretan, L.; and Berg, O. E.: Review of Direct Measurements of Interplanetary Dust from Satellites and Probes. Goddard Space Flight Center Contributions to the Cospar Meeting, May 1962. NASA TN D-1669, 1963, pp. 39-60.

3. Golovin, M. N.; and Putnam, A. A.: The Inertial Impaction of Small Particles. Rept. No. TN 58-36, Arnold Eng. Dev. Center, June 1958.

4. Marble, Frank E.: Dynamics of a Gas Containing Small Solid Particles. Combustion and Propulsion, R. P. Hagerty, et al., eds., Pergamon Press, 1963, pp. 175-213; Discussion, pp. 213-215.

5. Rudinger, George: Dynamics of Gas-Particle Mixtures with Finite Particle Volume. Paper No. 65-9, AIAA, 1965.

6. Mirels, H.; and Braun, W. H.: Nonuniformities in Shock-Tube Flow Due to Unsteady-Boundary-Layer Action. NACA TN 4021, 1957.

7. Roshko, Anatol: On Flow Durations in Low-Pressure Shock Tubes. Phys. Fluids, vol. 3, no. 6, Nov.-Dec. 1960, pp. 835-842.

8. Glass, I. I.: Shock Tubes. Pt. I - Theory and Performance of Simple Shock Tubes. Rev. No. 12, Univ. of Toronto, May 1958.

9. Laurence, J. C.; and Sandborn, V. A.: Heat Transfer from Cylinders. Symposium on Measurements in Unsteady Flow, Worchester (Mass.), May 21-23, 1962, pp. 36-43.

10. Anon.: Kodak Plates and Films for Science and Industry. Pub. No. 9, Eastman Kodak Co., 1962.

11. Camm, John C.; and Rose, Peter H.: Electric Shock Tube for High Velocity Simulation. Res. Rept. No. 136, Avco-Everett Res. Lab., July 1962.

12. Rudinger, G.: Experiments on Shock Relaxation in Particle Suspensions in a Gas and Preliminary Determination of Particle Drag Coefficients. Rept. No. CAL-90-P, Cornell Aero. Lab., July 1963.

13. Crowe, C. T.; Nicholls, J. A.; and Morrison, R. B.: Drag Coefficients of Inert and Burning Particles Accelerating in Gas Streams. Ninth Symposium (International) on Combustion, Academic Press, Inc., 1963, pp. 395-406.

14. Summers, James L.: Investigation of High-Speed Impact: Regions of Impact and Impact at Oblique Angles. NASA TN D-94, 1959.

15. Herrmann, Walter; and Jones, Arfon H.: Survey of Hypervelocity Impact Information. Rept. No. 99-1, M.I.T., Sept. 1961.

16. Eichelberger, R. J.; and Gehring, J. W.: Effects of Meteoroid Impacts on Space Vehicles. BRL Rept. No. 1155, Aberdeen Proving Ground, Dec. 1961.

17. Mark, Herman; Sommers, Ralph D.; and Mirtich, Michael J.: Effect of Surface Thermal Properties of Calibrated Exposure to Micrometeoroid Environment. Paper No. 65-138, AIAA, 1965.

18. McAdams, W. H.: Heat Transmission. Third Edition, McGraw-Hill Book Co., Inc., 1954.

NASA-Langley, 1966 E-3039

"The aeronautical and space activities of the United States shall be conducted so as to contribute . . . to the expansion of human knowledge of phenomena in the atmosphere and space. The Administration shall provide for the widest practicable and appropriate dissemination of information concerning its activities and the results thereof."

—NATIONAL AERONAUTICS AND SPACE ACT OF 1958

NASA SCIENTIFIC AND TECHNICAL PUBLICATIONS

TECHNICAL REPORTS: Scientific and technical information considered important, complete, and a lasting contribution to existing knowledge.

TECHNICAL NOTES: Information less broad in scope but nevertheless of importance as a contribution to existing knowledge.

TECHNICAL MEMORANDUMS: Information receiving limited distribution because of preliminary data, security classification, or other reasons.

CONTRACTOR REPORTS: Technical information generated in connection with a NASA contract or grant and released under NASA auspices.

TECHNICAL TRANSLATIONS: Information published in a foreign language considered to merit NASA distribution in English.

TECHNICAL REPRINTS: Information derived from NASA activities and initially published in the form of journal articles.

SPECIAL PUBLICATIONS: Information derived from or of value to NASA activities but not necessarily reporting the results of individual NASA-programmed scientific efforts. Publications include conference proceedings, monographs, data compilations, handbooks, sourcebooks, and special bibliographies.

Details on the availability of these publications may be obtained from:

SCIENTIFIC AND TECHNICAL INFORMATION DIVISION

NATIONAL AERONAUTICS AND SPACE ADMINISTRATION

Washington, D.C. 20546